Density Functional Theory Study on the Structural and Electronic Properties of Low Index Rutile Surfaces for $TiO_2/SnO_2/TiO_2$ and $SnO_2/TiO_2/SnO_2$ Composite Systems†

A. Beltrán,*,‡ J. Andrés,‡ J. R. Sambrano,‡,§ and E. Longo||

Departament de Química Física i Analítica, Universitat Jaume I, Campus de Riu Sec, Castelló E-12071, Spain, Grupo de Modelagem e Simulação Molecular, DM, Universidade Estadual Paulista, P.O. Box 473, 17033-360 Bauru, São Paulo, Brazil, and LIEC, Instituto de Química, Universidade Estadual Paulista, P.O. Box 355, 14801-907, Araraquara, São Paulo, Brazil

Received: February 23, 2008; Revised Manuscript Received: June 26, 2008

The present study is concerned with the structural and electronic properties of the $TiO_2/SnO_2/TiO_2$ and $SnO_2/TiO_2/SnO_2$ composite systems. Periodic quantum mechanical method with density functional theory at the B3LYP level has been carried out. Relaxed surface energies, structural characteristics and electronic properties of the (110), (010), (101) and (00) low-index rutile surfaces for $TiO_2/SnO_2/TiO_2$ and $SnO_2/TiO_2/SnO_2$ models are studied. For comparison purposes, the bare rutile TiO_2 and SnO_2 structures are also analyzed and compared with previous theoretical and experimental data. The calculated surface energy for both rutile TiO_2 and SnO_2 surfaces follows the sequence (110) < (010) < (101) < (001) and the energy increases as (010) < (101) < (110) < (001) and (010) ≈ (110) < (101) < (001) for $SnO_2/TiO_2/SnO_2$ and $TiO_2/SnO_2/TiO_2$ composite systems, respectively. $SnO_2/TiO_2/SnO_2$ presents larger values of surface energy than the individual SnO_2 and TiO_2 metal oxides and the $TiO_2/SnO_2/TiO_2$ system renders surface energy values of the same order that the TiO_2 and lower than the SnO_2. An analysis of the electronic structure of the $TiO_2/SnO_2/TiO_2$ and $SnO_2/TiO_2/SnO_2$ systems shows that the main characteristics of the upper part of the valence bands for all the studied surfaces are dominated by the external layers, i.e., by the TiO_2 and the SnO_2, respectively, and the topology of the lower part of the conduction bands looks like the core layers. There is an energy stabilization of both valence band top and conduction band bottom for (110) and (010) surfaces of the $SnO_2/TiO_2/SnO_2$ composite system in relation to their core TiO_2, whereas an opposite trend is found for the same surfaces of the $TiO_2/SnO_2/TiO_2$ composite system in relation to the bare SnO_2. The present theoretical results may explain the growth of $TiO_2@SnO_2$ bimorph composite nanotape.

I. Introduction

The design and preparation of nanocomposites based on semiconducting oxides is an important goal for the obtainment of improved functional performances in advanced fields such as optoelectronics, sensing, and catalysis.[1−9] Recently, mixed metal oxides or binary semiconducting systems have attracted more and more attention and some researchers pointed out that they were promising candidates for the fabrication of materials showing novel technological applications thanks to the possibility of achieving a synergistic combination, which are often superior to those of the component characteristics.[10−14]

Particularly, systems based on both rutile TiO_2 and SnO_2 surfaces are a fascinating class of materials in terms of the electronic and optical properties and they are prepared and characterized by surface science techniques[15−19] and studied by means of theoretical methods.[20−33] The coupling of TiO_2 with SnO_2 can affect the electronic structure and can thus be used to control and enhance to some extent the surface chemical and physical properties of these systems.

Lee and Hwang[17] investigated the fabrication of SnO_2/TiO_2 thin films to obtain an appropriate substrate material for oxygen gas sensors. The electronic properties of TiO_2/SnO_2 layers[34,35] as well as the optoelectronic properties of the TiO_2/SnO_2 junctions have been also reported by Kunst et al.[36] Akurati et al.[37] synthesized TiO_2/SnO_2 composite nanoparticles and tested their photocatalytic activity for the degradation of methylene blue. A coupled photocatalysts SnO_2/TiO_2 was prepared by Chen and co-workers.[38] For these authors the improved photocatalytic activity may be attributed to the enhance charge separation efficiency and extend the wavelength range of photoexcitation. Liu et al. showed that the photocatalytic efficiency of a TiO_2 catalyst was enhanced by adding SnO_2 onto TiO_2.[39] Ohsaki and co-workers[35] investigated the photocatalytic activity of TiO_2 overcoated with SnO_2. They found that the interface between TiO_2 and SnO_2 acts as a potential barrier for the carriers photogenerated in TiO_2 and the photogenerated species pass through the SnO_2 overlayer depending on the SnO_2 film characteristics. SnO_2 nanoparticles in the rutile phase were loaded by Chai et al.[40] on the surface of TiO_2 to form SnO_2/TiO_2 nanocomposite structure. The SnO_2/TiO_2 with 1 mol % SnO_2 demonstrated 1.5−1.7 times of photocatalytic activity compared to the pure TiO_2 in decomposing gaseous 2-propanol and in evolving CO_2. The role of SnO_2 nanoparticles on TiO_2 surface is considered to be retardation of recombination rate between electrons and holes by trapping the photoexcited

† Part of the special section for the "Symposium on Energetics and Dynamics of Molecules, Solids and Surfaces".

* Corresponding author. E-mail address: beltran@uji.es.

‡ Universitat Jaume I.

§ Grupo de Modelagem e Simulação Molecular, DM, Universidade Estadual Paulista.

|| Instituto de Química, Universidade Estadual Paulista.

10.1021/jp801604n CCC: $40.75
Published on Web 08/05/2008

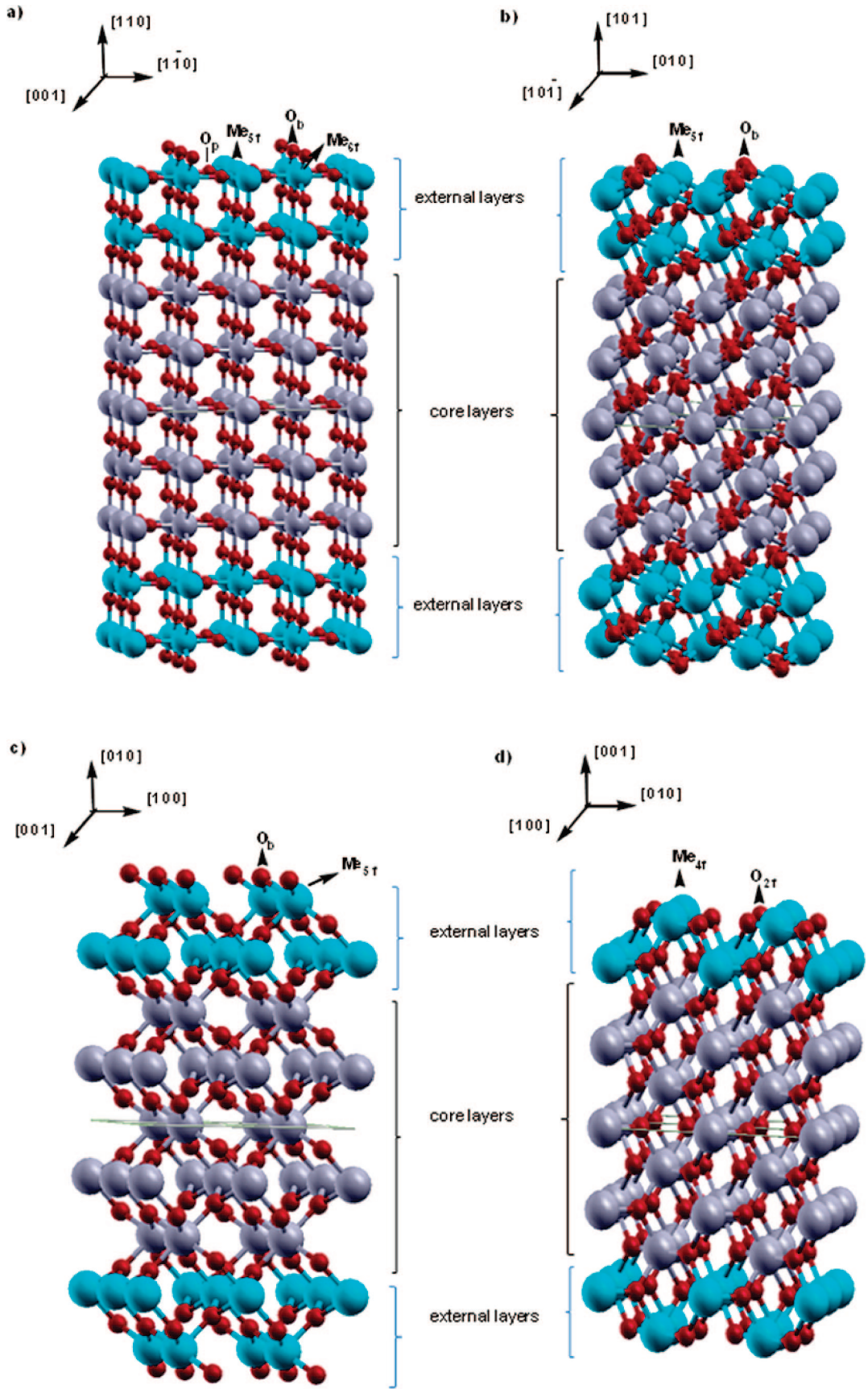

Figure 1. Schematic representation of the four surface models (a) (110), (b) (101), (c) (010) and (d) (001) and the corresponding directions for the four studied systems. The atomic labels Me (Ti or Sn) and O are shown for the most external surface positions.

electrons from the conduction band of TiO_2. Tada et al.[41] demonstrates that the sol−gel patterned TiO_2 films formed on SnO_2-film coated Soda Lime-glass exhibit very high levels of photocatalytic activity for both gas and liquid phase reactions. These authors comment the efficient interfacial electron transfer from the TiO_2 overlayer to the SnO_2 underlayer.

TABLE 1: Thickness Values (Å), after Relaxation, for the Core and Both External Layers of Different Surfaces of $SnO_2/TiO_2/SnO_2$ and $TiO_2/SnO_2/TiO_2$ Model Systems

	$SnO_2/TiO_2/SnO_2$		$TiO_2/SnO_2/TiO_2$	
surface	core TiO_2	external SnO_2	core SnO_2	external TiO_2
(110)	17.28	6.90	15.95	6.36
(010)	10.99	6.38	11.23	4.46
(101)	11.45	5.38	12.00	4.90
(001)	9.38	3.28	9.81	2.94

TABLE 4: Atomic Displacements, Δx, Δy and Δz (Å), and Mulliken Charges, Q (in \|e\|), for the (010) Surface Systems[a]

	O_b			Me_{5f}		
	Δy	Δz	Q	Δy	Δz	Q
TiO_2	−0.31	0.04	−0.66	0.10	−0.03	1.53
$SnO_2/TiO_2/SnO_2$	−0.21	0.43	−0.81	0.05	0.24	1.93
SnO_2	−0.27	0.14	−0.84	0.06	0.02	1.92
$TiO_2/SnO_2/TiO_2$	−0.36	−0.22	−0.71	0.13	−0.21	1.58

[a] Δx for all the atomic positions is negligible.

The results reported by Ribeiro et al.[42] are focused on the growth mechanism in the formation of TiO_2/SnO_2 heterostructures. Pulsed laser ablation was used to deposit TiO_2 onto a SnO_2 nanoribbon to yield composite TiO_2@SnO_2 nanotapes.[43] Recently, Hou et al.[44] synthesized SnO_2/TiO_2 nanotube composite photocatalysts with different SnO_2 contents by means of a solvothermal process, and Liu et al.[45] reported a simple approach for fabricating bicomponent TiO_2/SnO_2 nanofibers with controllable heterojunctions. Both of the TiO_2 and SnO_2 components in the nanofibers are fully exposed to the surface. This morphology fully utilized the photogenerated holes and electrons during the photocatalytic process, thus leading to a high photocatalytic activity.

Zakrzewska et al. carried out extensive studies on TiO_2-SnO_2 system for gas sensing[46−48] and they found, on the basis of atomic force microscopy and transmission electron microscopy studies, that the grain size and the surface roughness of thin films were affected by the chemical composition of TiO_2-SnO_2. In addition, they note that the band gap (BG) increases systematically from that of TiO_2 to that of SnO_2 upon variation of the composition. These results agree with previous calculations reported by us.[49,50] In our study on TiO_2-SnO_2 solid solution[49] we found that the Sn substitution for Ti in rutile increases the oxidation−reduction potential of the oxide and renders the lowest energy transition to be indirect. These effects are believed to inhibit the photogenerated electron−hole recombination, and thus endow the enhanced photoactivity for $Sn_xTi_{1-x}O_2$ solid solutions.

Compared with bare TiO_2 and SnO_2 metal oxides, both $SnO_2/TiO_2/SnO_2$ and $TiO_2/SnO_2/TiO_2$ composite systems have not received the same theoretical attention, and to our knowledge, the electronic structures of these systems have not been reported despite the broad interest and their importance. The motivation of this work was to shed light, at the atomic level, on the surface and electronic structures of these composite systems. This study was mainly based on the first-principles method in conjunction with slab models. It is then of interest to learn how stability is related to electronic structure, in terms of optimized geometric parameters, band-structure analyses, and the redistributions of charge density. Finally, for comparison purposes, the bare TiO_2 and SnO_2 surfaces have been also studied.

II. Theoretical Methods and Model Systems

Calculations were performed with the CRYSTAL06 program package.[51] For the titanium atom, the 6-31G basis set developed by Rassolov et al.[52] was selected, as in previous papers.[27,53,54] Oxygen and tin centers have been described by the standard 6-31G* basis set and in the scheme PS-21G*,[55] respectively, where PS stands for Durand−Barthelat's nonrelativistic large effective core potential.[56] Becke's three-parameter hybrid nonlocal exchange functional[57] combined with the Lee−Yang−Parr gradient-corrected correlation functional, B3LYP,[58] has been used. Hybrid density functional methods have been extensively used for molecules and provide also an accurate description of crystalline structures as bond lengths, binding energies, and BG values are regarded.[59] The diagonalization of the Fock matrix was performed at adequate k-point grids in the reciprocal space being the Pack−Monkhorst/Gilat shrinking factors IS = ISP = 4. The thresholds controlling the accuracy of the calculation of Coulomb and exchange integrals were set to 10^{-8} (ITOL1 to ITOL4) and 10^{-14} (ITOL5), whereas the percent of Fock/Kohn−Sham matrices mixing was set to 40 (IPMIX = 40).[51]

Full optimization of the cell parameters (a and c) and internal coordinate (u) for the bulk SnO_2 and TiO_2 systems have been carried out. In this work we report the results for

TABLE 2: Cell Parameters, a and c (in Å), Oxygen Fractional Coordinate (u) and Band Gap Energy, E_g (eV), for Bare TiO_2 and SnO_2[a]

	TiO_2				SnO_2			
	a	c	u	E_g	a	c	u	E_g
this work	4.6055	3.0040	0.3051	3.31	4.7250	3.1657	0.3062	3.61
exp	4.5936	2.9587	0.3048	3.06[iii]-3.0[iv]	4.737	3.186	0.306	3.6[vi]
B3LYP[i,ii]	4.6400	2.9683	0.3051	3.24[v]	4.718	3.187	0.307	3.51[vii]

[a] TiO_2 references: i = ref 50, iii = ref 70, iv = refs 71−73, v = ref 27. SnO_2 references: ii = ref 60, vi = refs 26, 60, 74−78, vii = ref 79.

TABLE 3: Atomic Displacements, Δx, Δy and Δz (Å), and Mulliken Charges, Q (in \|e\|), for the (110) Surface Systems[a]

	O_b		Me_{6f}		Me_{5f}		O_p		
	Δz	Q	Δz	Q	Δz	Q	Δy	Δz	Q
TiO_2	0.06	−0.67	0.28	1.58	−0.15	1.66	−0.04	0.17	−0.84
$SnO_2/TiO_2/SnO_2$	0.42	−0.86	0.45	2.15	−0.14	2.10	−0.03	0.32	−1.10
SnO_2	0.07	−0.90	0.20	2.09	−0.13	2.05	−0.06	0.13	−1.05
$TiO_2/SnO_2/TiO_2$	−0.30	−0.72	0.03	1.63	−0.33	1.67	−0.06	−0.05	−0.85

[a] Δx for all the atomic positions and Δy for O bridge and Me (6-fold and 5-fold) are negligible.

TABLE 5: Atomic Displacements, Δx, Δy and Δz (Å), and Mulliken Charges, Q (in \|e\|), for the (101) Surface Systems

	O_b				Me_{5f}			
	Δx	Δy	Δz	Q	Δx	Δy	Δz	Q
TiO_2	−0.12	−0.08	−0.07	−0.71	0.19	0.11	−0.08	1.53
$SnO_2/TiO_2/SnO_2$	0.12	0.26	0.35	−0.88	0.14	0.20	0.24	1.95
SnO_2	0.03	0.00	0.02	−0.88	0.18	0.03	0.00	1.92
$TiO_2/SnO_2/TiO_2$	−0.15	−0.20	−0.25	−0.73	0.16	0.16	−0.18	1.54

TABLE 6: Atomic Displacements, Δx, Δy and Δz (Å), and Mulliken Charges, Q (in \|e\|), for the (001) Surface Systems[a]

	Me_{4f}		O_{2f}			
	Δz	Q	Δx	Δy	Δz	Q
TiO_2	−0.26	1.38	−0.09	0.09	0.03	−0.72
$SnO_2/TiO_2/SnO_2$	−0.02	1.67	−0.06	0.06	0.29	−0.86
SnO_2	−0.21	1.66	−0.08	0.08	0.11	−0.86
$TiO_2/SnO_2/TiO_2$	−0.41	1.48	−0.10	0.10	−0.16	−0.75

[a] Δx and Δy for the Me_{4f} atomic positions is negligible in all systems.

the low index (110), (101), (100) and (001) surfaces and for this purpose these surfaces of both bare SnO_2 and TiO_2 metal oxides as well as the $SnO_2/TiO_2/SnO_2$ and $TiO_2/SnO_2/TiO_2$ composite systems have been modeled by unreconstructed (truncated bulk) slab models using the calculated equilibrium geometry. As these surfaces have different numbers of atoms in each layer, the low-index surfaces were modeled with different thicknesses in the z-direction but were periodic in the x- and y-directions. To confirm the convergence of the total energy with respect to slab thickness of the different surface models, we calculate the surface energy for the four different surfaces. The values are converged in the range 0.031 (0.020), 0.006 (0.091), 0.001 (0.011) and 0.054 (0.009) J m^{-2} for TiO_2 (and SnO_2) slab models containing nine trilayers for the 110, 010 and 101 surfaces and eleven layers for the 001, respectively. On the other hand, the band gap values are converged to better than 0.04 eV for both bare SnO_2 and TiO_2 slab models.

It is worth noting that, at variance with the procedure adopted in the plane waves codes, our slab model does not include images above and below the reference slab and the system is a true bidimensional crystal. Internal degrees of freedom have been optimized for both the external and core layers of each slab.

Figure 1 schematizes the four studied surface models for bare TiO_2 and SnO_2 as well as $SnO_2/TiO_2/SnO_2$ and $TiO_2/SnO_2/TiO_2$ composite systems including the corresponding atomic labels. Values of the thickness, after relaxation, of the core and both external layers for $SnO_2/TiO_2/SnO_2$ and $TiO_2/SnO_2/TiO_2$ model systems are reported in Table 1.

The band structures have been obtained along the appropriate high-symmetry paths of the Brillouin zone. For the 2D Brillouin those paths are the same used by Mäki-Jaskari and Rantala[23] and also by us in a previous work.[50]

III. Results and Discussion

IIIa. Bulk Properties. The structural parameters and the BG values for SnO_2 and TiO_2 are reported in Table 2. There is good agreement between the present results, experimental data and those obtained in our previous studies,[49,50,60] performed with the same basis set for Ti but slightly different for Sn and O centers.

IIIb. Surface Geometry. Geometrical displacements and Mulliken charges for the (110), (010), (101) and (001) surfaces are summarized in Tables 3, 4 and 6, respectively. Figure 1 shows that the (110) surface has metal atoms yielding coordination six (Me_{6f}) and five (Me_{5f}) and two kinds of oxygen atoms, bridge atom (O_b) and in-plane atom (O_p). The (101) surface exhibits two kinds of atoms, 5-fold, Me_{5f}, and 2-fold coordinated, O_{2b}. For the (010) surface, the first two atomic layers exhibit O_b and Me_{5f} atoms, respectively. In the (001) surface, there is 4-fold (Me_{4f}) and 2-fold (O_{2f}) coordinated atoms.

In our models the top and bottom slabs are equivalent by symmetry. Although TiO_2 is isostructural to SnO_2 the lattice mismatch is substantial $(a_{SnO_2} - a_{TiO_2})/a_{TiO_2} = (4.73 - 4.61)/4.61 = 2.6\%$ and $(c_{SnO_2} - c_{TiO_2})/c_{TiO_2} = (3.17 - 3.00)/3.00 = 5.4\%$ and consequently the interface between substrate and film has to accommodate this lattice mismatch. Relaxed positions of the atoms on all the surfaces studied in the x-, y- and z-directions, Δx, Δy and Δz being the difference between bulk-truncated and relaxed positions. The positive displacements in the z-direction, Δz, denote relaxations toward the vacuum region and the negative displacement denote relaxations inward the bulk. When Δx, Δy are close to zero, they are not included in the corresponding tables.

For the $TiO_2/SnO_2/TiO_2$ (110) surface the displacements of the O_b, O_p and Ti_{5f} in the z-direction are inward (see Table 3); on the other hand, for the Ti_{6f} Δz displacements the corresponding values are positive, toward the vacuum region, and the values for bare TiO_2 (110) surface are always positive except for the Ti_{5f} atoms, where there is an overall decrease in the surface corrugation. For the $SnO_2/TiO_2/SnO_2$ (110) surface, the relaxation in the z-direction is positive and larger than that for the bare SnO_2 for the O_b, O_p and Sn_{6f} atoms, and negative but with a lower value than for the Sn_{5f} atoms. The Δx and Δy displacements are negligible or very small (O_p).

An analysis of the results presented in Tables 4−6 shows that there are pronounced displacements outward for O_b ((010) and (101) surfaces) and O_{2f} (001) as well as for Sn_{5f} ((010) and (101) surfaces) whereas for the Sn_{4f} (001) $SnO_2/TiO_2/SnO_2$ surface there is a slight inward displacement of −0.02 Å. For the $TiO_2/SnO_2/TiO_2$ equivalent systems negative Δz displacements relative to the bare SnO_2 are found; all the oxygen and titanium atoms present inward displacements except the Sn_{6f} atoms of the (110) surface that shows a slight outward displacement of 0.03 Å.

The relaxation of (010) surfaces, shown in Table 4, gives noticeable negative displacements in the y-direction for the oxygen bridge (O_b) in all the systems, Δx for all the atomic positions being negligible. Table 5 shows the atomic displacements for the first and second layers of the (101) surface systems. Bare TiO_2 presents negative and positive displacements along the x-direction for O_b for Ti_{5f} atoms, respectively; the same behavior is found for the corresponding $TiO_2/SnO_2/TiO_2$ surface. For the SnO_2 and $SnO_2/TiO_2/SnO_2$ systems the corresponding Δx displacements are positive for the O_b and Ti_{5f} atoms, respectively. O_b Δy displacements become negative in the TiO_2 and $TiO_2/SnO_2/TiO_2$ systems,

TABLE 7: Unrelaxed ($E_{surf}^{unrelax}$) and relaxed (E_{surf}^{relax}) Surface Energies (J m^{-2}) for Several Low Index Planes, and the Corresponding Band Gap Energy, E_g (eV)[a]

	TiO_2				$SnO_2/TiO_2/SnO_2$				SnO_2				$TiO_2/SnO_2/TiO_2$			
surface	(110)	(010)	(101)	(001)	(110)	(010)	(101)	(001)	(110)	(010)	(101)	(001)	(110)	(010)	(101)	(001)
$E_{surf}^{unrelax}$	1.73	1.82	1.90	2.75	4.11	3.59	3.96	4.15	2.04	2.15	2.57	3.34	2.15	2.22	2.33	3.24
E_{surf}^{relax}	0.67	0.94	1.19	1.59	3.23	2.78	2.93	3.30	1.56	1.74	2.11	2.71	0.78	0.77	1.04	1.57
b	0.47−0.17	0.60−0.28	0.95−0.43	0.64−0.44					1.04	1.14	1.33	1.72				
c	0.89	1.12	1.40	1.65					1.38−1.40	1.65−1.66	1.55	2.36				
d	0.48−0.54	0.67−0.76	1.01−1.08	1.21−1.32					1.20	1.27	1.43	1.84				
E_g	3.24[D]	3.46[D]	3.44[D]	3.19[I*#]	2.57[I**]	3.55[I]	3.22[D]	2.76[D]	2.68[I**]	3.55[I]	2.77[D]	2.53[D]	3.70[D]	3.75[D]	3.70[D]	3.48[D]

[a] D is the direct BG. I is the indirect BG. Key: D = direct (Γ→Γ); I = indirect (M→Γ); I* = indirect (Γ→M); I** = indirect (~X →Γ) ~X = point is located in the path between X and Γ; # = 3.32[D]; [b] TiO_2,[22,67] SnO_2.[22] [c] TiO_2,[21,80] SnO_2.[81] [d] TiO_2,[68] SnO_2.[66]

and positive in the $SnO_2/TiO_2/SnO_2$ and SnO_2 cases. Me_{5f} Δy displacements are always positive, being more important in the $SnO_2/TiO_2/SnO_2$ and $TiO_2/SnO_2/TiO_2$ systems. Finally, in Table 6 we can see that the O_{2f} Δx and Δy displacements in the (001) surface are negative and positive, respectively in all systems.

The relaxation of bare TiO_2 (110) surface has been recently restudied both experimentally and theoretically, and our results are in agreement with the most recent bibliography.[24,61,62] SnO_2 (110) surfaces also give displacements of the same range that those reported by previous studies.[24,50,63] The results of Mulliken population analysis for the four surfaces listed in Tables 3−6 indicate that the values of positive and negative charge on metal and oxygen atoms, respectively, are larger for bare SnO_2 and $SnO_2/TiO_2/SnO_2$ systems than for bare TiO_2 and $TiO_2/SnO_2/TiO_2$ models.

IIIc. Surface Energy. The standard method for calculating the surface energy, E_{surf}, is based on the general expression

$$E_{surf} = \lim_{N\to\infty} \frac{E^N(\text{slab}) - nE(\text{bulk}) - n'E(\text{bulk}')}{2A} \quad (1)$$

where E(bulk) is the total energy of bulk TiO_2 or/and SnO_2 per unit formula, E^N(slab) is the energy of the slab containing n layers of TiO_2 and/or n' layers of SnO_2 units, with $n + n' = N$; A is the area of the unit cell, and the factor 2 comes from the fact that each slab has two surfaces. To calculate E(bulk), two approaches can be used: (i) E(bulk) can be obtained from the slope of the slab total-energy data versus N, as it was proposed by Fiorentini and Methfessel[64] and later applied by Marlo and Milma.[65] (ii) E(bulk) can be calculated from bulk crystal calculations. When the number of layers N becomes large and convergence is approached, E_{surf} can be calculated as follows:

$$E_{surf} \approx \frac{E^N(\text{slab}) - nE(\text{bulk}) - n'E(\text{bulk}')}{2A} \quad (2)$$

Although the linear behavior in the calculated surface energy can be already prominent for thicknesses of seven or more layers, using slab thicknesses of nine or eleven MO2 layers the differences in energy between different surfaces are clear, the reported calculations can be considered reasonably reliable from a qualitative point of view and the general trends correct. This procedure has been used in the present work and in previous studies of our group[27,53,66] and other workers.[21,22,67,68]

Unrelaxed ($E_{surf}^{unrelax}$) and relaxed (E_{surf}^{relax}) surface energies of the low index studied planes, compared with experimental and some theoretical values, and the corresponding energy gap, E_g, values with a direct or indirect character are showed in Table 7. Assuming that the error due to the exchange and correlation functional is systematic to all the surfaces, not greatly affecting the relative energies of two different surfaces, it is still possible to extract some trends from our results.

The calculated energy increasing order is (110) < (010) < (101) < (001) and the values of surface energy for different rutile TiO_2 surfaces obtained by means of B3LYP computing level are similar with other theoretical studies carried by Ramamoorthy et al. using the DFT-LDA method[21] and by Perron et al. using the GGA-PAW method,[68] whereas lower values of surface energy are reported by Barnard et al.[67] The calculated values of surface energy for SnO_2 surfaces follow the same energy increasing sequence that those reported by Oviedo and Gillan[22] and our previous study.[66] It is apparent that the relaxation of the atoms on the surface decreases significantly the calculated surface energies. As expected,

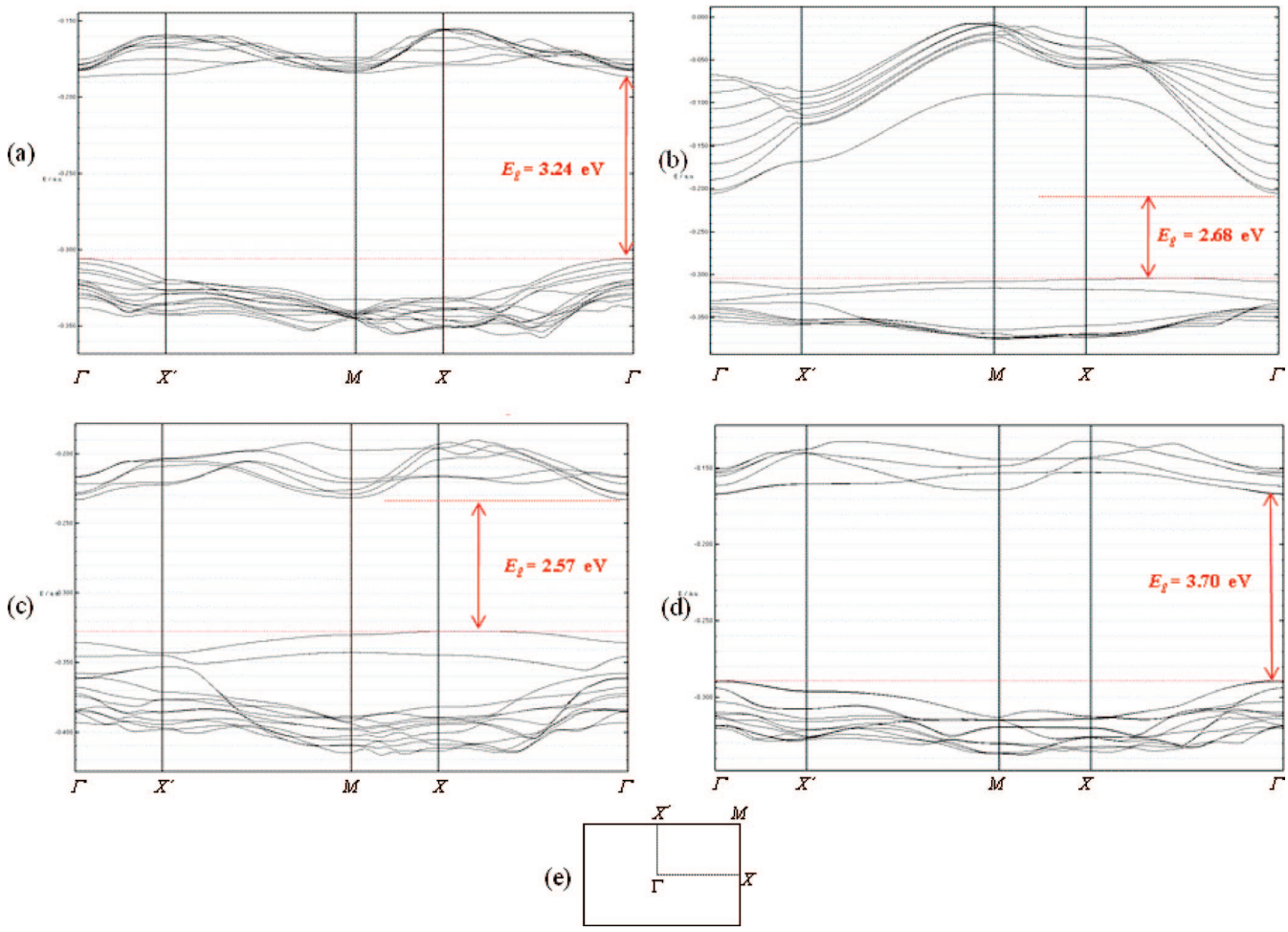

Figure 2. Band structure of the (110) surfaces: TiO_2 (a); SnO_2 (b); $SnO_2/TiO_2/SnO_2$ (c); $TiO_2/SnO_2/TiO_2$ (d). The first Brillouin zone with high symmetry points for the surfaces is also shown (e).

surface energies appear to be related to the presence of undercoordinated Me and O atoms.

The results shown in Table 7 indicate that the surfaces with 4-fold-coordinated Me (i.e., the (001) ones) have a larger energy than those with 5-fold-coordinated Me (the rest). Furthermore, the surface energy (of the relaxed structure) approximately increases with the increase of the density of undercoordinated Me atoms.

The composite $SnO_2/TiO_2/SnO_2$ system exhibits much higher surface energy than the bare SnO_2 and TiO_2 systems whereas the $TiO_2/SnO_2/TiO_2$ one presents surface energy values of the same order and lower than the bare TiO_2 and SnO_2 systems, respectively. For the $SnO_2/TiO_2/SnO_2$ model the calculated energy increasing sequence is (010) < (101) < (110) < (001) and an inversion in the order is found between the (110) and (010) surfaces when compared with the bare SnO_2 and TiO_2 systems, the (010) surface being the most stable by 0.52 J m^{-2} before and 0.45 J m^{-2} after relaxation than the (110) one. In this case, the relaxation process decreases the surface energy of the (110) and (010) systems by 21% and 23%, respectively. On the other hand, the (101) surface energy is 0.15 J m^{-2} before and 0.30 J m^{-2} after relaxation, lower than the (110) one, and the relaxation diminishes the energy by 26%. The gain of stability of (010) and (101) surfaces in relation to (110) can be associated with their more open ((010)) and corrugated ((010) and (101)) structures in which the large Sn atoms of the SnO_2 layer can be accommodated better on the TiO_2 core. As we can see in Table 1, the wide of the external slabs in $SnO_2/TiO_2/SnO_2$ system are 6.38, 5.38 and 6.90 Å for the (010), (101) and (110) surface models, respectively.

For the $TiO_2/SnO_2/TiO_2$ model, the relaxation process decreases the surface energy of the (110) and (010) by 64% and 65%, respectively, and the difference in energy between the (110) and (010) surfaces is only 0.07 J m^{-2} before, and −0.01 J m^{-2} after relaxation; then the stability energy sequence is (010) ≈ (110) < (101) < (001) and the TiO_2 external slabs have a smaller thickness in the (010) surface, 4.46 Å, than in the (110) one, 6.36 Å (see Table 1).

Our results may explain the growth of the TiO_2@SnO_2 bimorph composite nanotape reported by He et al.[43] They obtained rutile SnO_2 single-crystalline nanoribbons with a [101] growth direction and well-faceted, nearly rectangular cross-sections bounded by (10$\bar{1}$) and (010) surface planes. Then, these atomically flat surface facets were appropriate substrates for the epitaxial growth of materials with appropriate crystal symmetries such as TiO_2, and high resolution transmission electron microscopy confirms that TiO_2 deposition results in an atomically sharp interface between TiO_2 and SnO_2. This nanotape has the TiO_2 epitaxially oriented on the narrow side (010) surface. These experimental data of He and co-workers[43] give credence to the theoretical predictions and allows us to be confident in our study.

IIId. Electronic Structure. An analysis of the results reported in Table 7 render that the bare TiO_2 surfaces present values of direct BG in the range from 3.24 to 3.46 eV, except in the (001) surface in which the BG is indirect with a value of 3.19 eV, the direct gap being 3.32 eV; the upper valence band

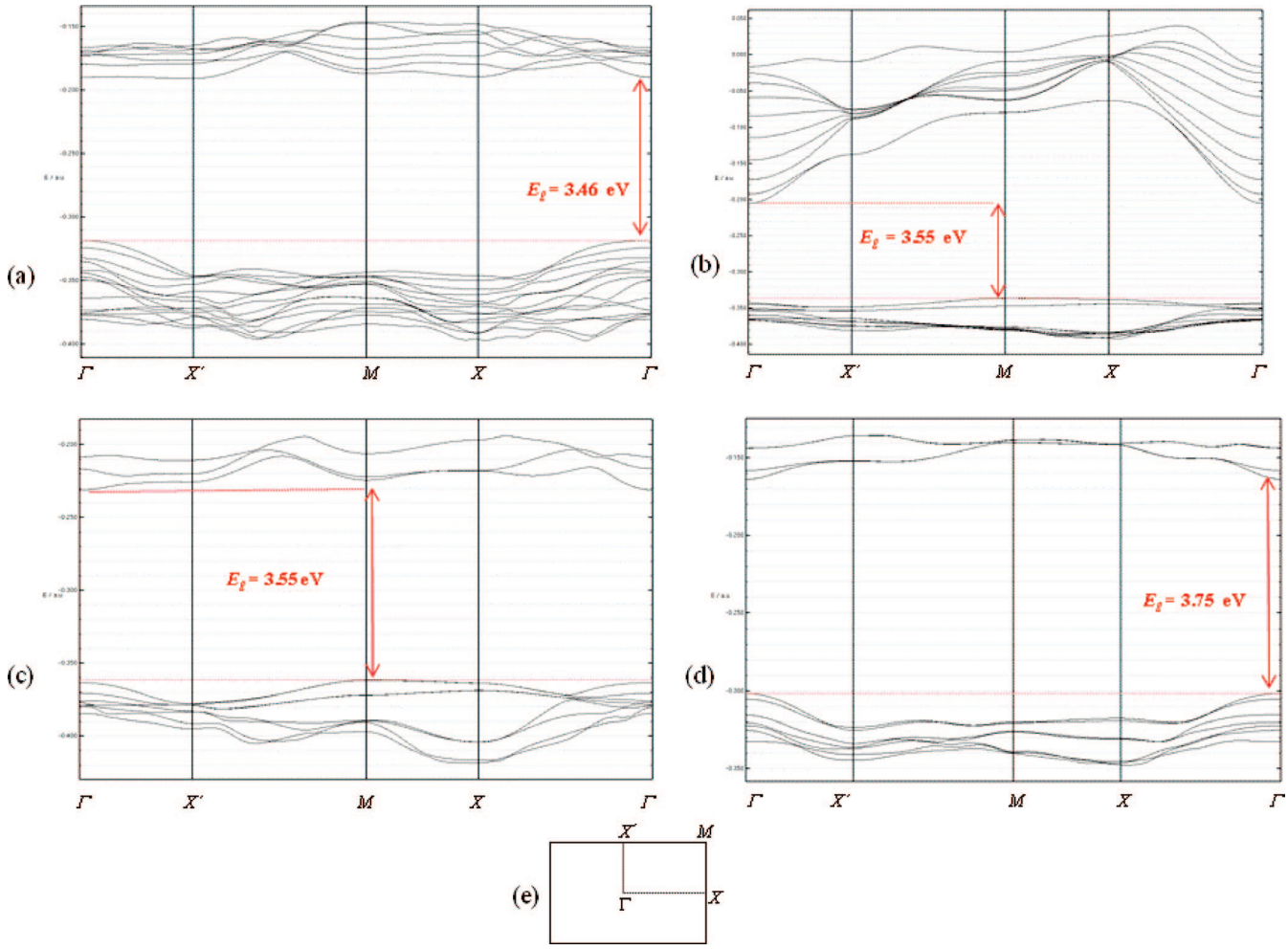

Figure 3. Band structure of the (010) surfaces: TiO_2 (a); SnO_2 (b); $SnO_2/TiO_2/SnO_2$ (c); $TiO_2/SnO_2/TiO_2$ (d). The first Brillouin zone with high symmetry points for the surfaces is also shown (e).

(VB) of the four surfaces is located at Γ. For the bare SnO_2 (110) surface the top of the VB is located in a point of the path between the X and Γ points, the bottom of the conduction band (CB) being at Γ, the gap of 2.68 eV is indirect, and the upper part of the VB is very flat in agreement with the band structure calculated by Mäki-Jaskari and Rantala.[23] The BG for the SnO_2 (010) surface is also indirect, between M and Γ points, its value being 3.55 eV. For the (101) and (001) surfaces the BG becomes direct at Γ, being 2.77 and 2.53 eV, respectively.

Our models for composite systems have two TiO_2 (or SnO_2) layers on both sides of each core composed of seven (nine in the (001) surfaces) SnO_2 (or TiO_2) layers. We have checked that, before the relaxation, the positions of the top of VB and the bottom of the CB do not change significantly when the amount of external layers is equal or larger than 2. The relative energy gap values do not change either. For the $SnO_2/TiO_2/SnO_2$ system, as in the bare SnO_2, the BG is direct in the (101) and (001) surfaces and indirect for the (110) and (010) ones. In the $TiO_2/SnO_2/TiO_2$ (110) surface the top of VB and the bottom of the CB are located at the Γ point, the direct gap being 3.70 eV. Lin and co-workers[69] found that the doping process of Ti on the SnO_2 (110) surface yields an indirect BG when the doped position is the 5-fold whereas the band gap is direct when the doped position is the 6-fold. In our model Ti atoms occupy both 5-fold and 6-fold positions and this fact can explain the discrepancy. All the remaining low index surfaces investigated of $TiO_2/SnO_2/TiO_2$ have direct BG. As commented above, the corresponding bare TiO_2 surfaces also present direct BG, except the (001) surface, but in this case the direct gap is close to the indirect one.

The band structures of the (110) and (010) surfaces are depicted in Figures 2 and 3, 5, respectively. An analysis of Figure 2 shows that the top of VB in the (110) surface has the following energy values: −8.31 eV (at Γ) for TiO_2, −8.26 eV (at ∼X) for SnO_2, −8.91 eV (at ∼X) for $SnO_2/TiO_2/SnO_2$ and −7.86 eV (at Γ) for $TiO_2/SnO_2/TiO_2$, and for the bottom of the CB the corresponding values are −5.08 eV (at Γ) for TiO_2, −5.58 eV (at Γ) for SnO_2, −6.34 eV (at Γ) for $SnO_2/TiO_2/SnO_2$ and −4.16 eV (at Γ) for $TiO_2/SnO_2/TiO_2$. In the $SnO_2/TiO_2/SnO_2$ (110) surface the BG is indirect (as in the bare SnO_2 (110) case) and its value is only of 2.57 eV, due to the low value of the energy of the bottom of the CB. The analysis of the corresponding projected density of states (PDOS) (not presented here) shows that the lower part of the CB has a dominant Ti 3d (core) character, with little contribution of Sn_{5f} 5s states and very little of O_p 2p states. The Sn_{5f} 5s and to a lesser extent O_p 2p states are predominant in the bottom of the CB of the bare SnO_2 (110) surface. On the other hand, the $TiO_2/SnO_2/TiO_2$ (110) surface presents a direct BG with an energy gap value of 3.70 eV due to the high value of the energy of the bottom of the CB, and the corresponding PDOS indicates that the lower part of the CB is mainly composed of the Ti_{5f} and Ti_{6f} 3d states and very little of O_p 2p states as in the TiO_2 (110) surface. In both coupled systems the upper VB is mainly composed of the O_b and O_p 2p states. The upper VB of both composite systems show the topology of the external layers.

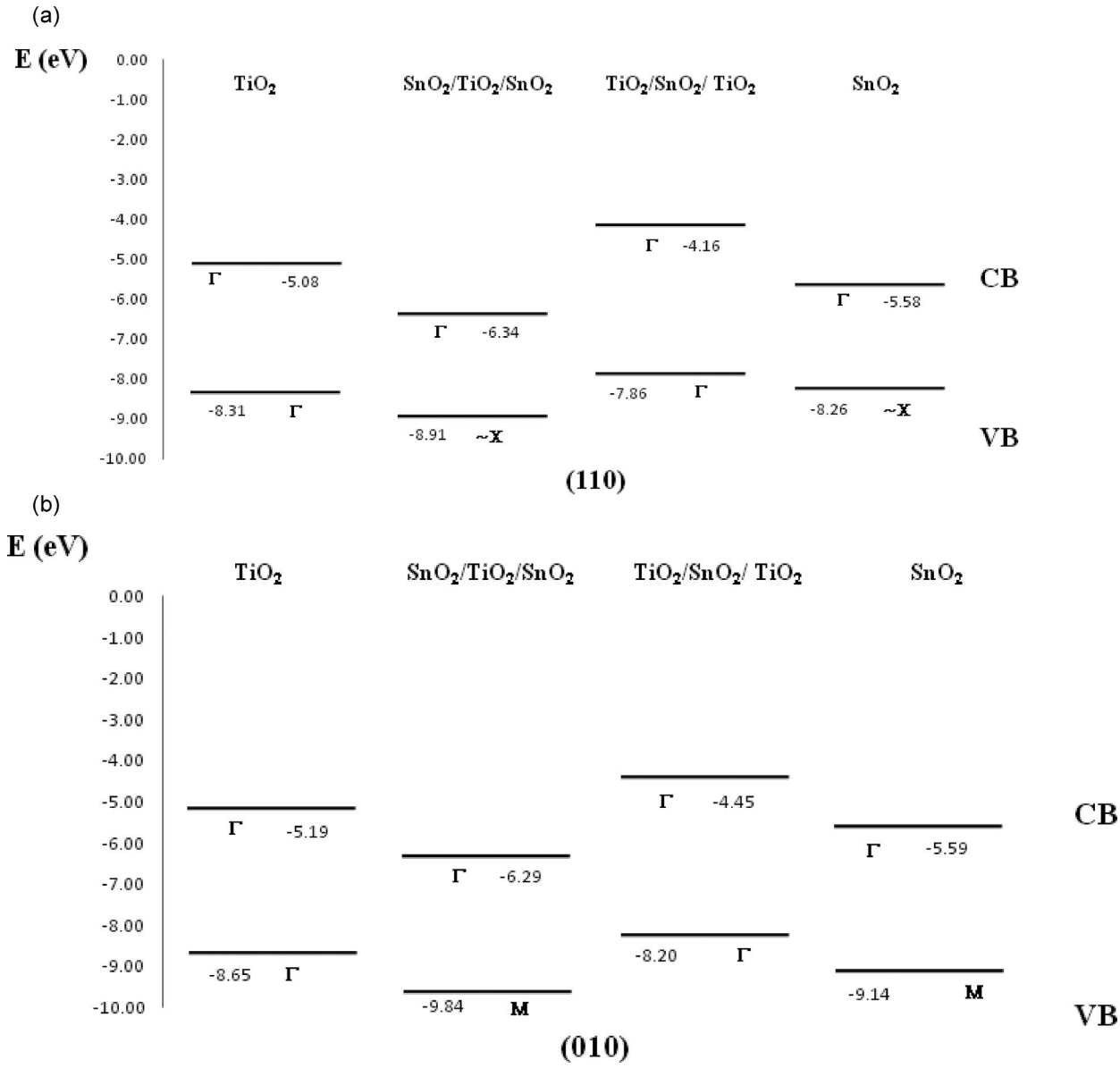

Figure 4. Schematic representation of the relative position of top of VB and the bottom of CB for the most stable a) (110) and b) (010) surface systems.

Figure 3 shows that the top of VB for theTiO_2 as well as the $TiO_2/SnO_2/TiO_2$ (010) surface is located at Γ having values of −8.65 and −8.20 eV, respectively, whereas for SnO_2 and $SnO_2/TiO_2/SnO_2$ it is located at M with values of −9.14 and −9.84 eV, respectively. The bottom of the CB in all systems is located at Γ with the following values: −5.19 eV (TiO_2), −6.29 eV ($SnO_2/TiO_2/SnO_2$), −5.59 eV (SnO_2) and −4.45 eV ($TiO_2/SnO_2/TiO_2$). An analysis of the PDOS for the $SnO_2/TiO_2/SnO_2$ system shows a dominant Ti 3d (core) character in the lower part of the CB, being the upper VB composed, as in the bare SnO_2 (010) surface, of O_b 2p states with little contribution of the Sn_{5f} 5s states. The PDOS analysis of the $TiO_2/SnO_2/TiO_2$ (010) system shows that the Ti_{5f} 3d and to a lesser extent the O_b 2p states are predominant in the lower part of CB, whereas the upper VB is composed mainly of the O_b 2p and Ti_{5f} 3d states, showing a clear resemblance with the corresponding bare TiO_2 system.

In the four studied surfaces the upper VB part present the characteristics of the external layers for $SnO_2/TiO_2/SnO_2$ and $TiO_2/SnO_2/TiO_2$ composite systems, whereas the lower part of the CB maintains the behavior of their respective cores, i.e., TiO_2 and SnO_2, respectively, and accordingly the direct or indirect character of the BG is mainly due to the external layers (see Table 7). Only the $TiO_2/SnO_2/TiO_2$ (001) surface presents a direct gap whereas for the corresponding bare TiO_2 (001) surface the energy gap is indirect.

The values of the BG for the four surfaces are affected in a different way by the presence of the external surface; i.e., there is a decrease of these values from bare TiO_2 to $SnO_2/TiO_2/SnO_2$ for the (110), (101) and (001) surfaces and an increase for the (010) one. On going from the bare SnO_2 to the $TiO_2/SnO_2/TiO_2$ systems, the BG values increase in all cases except for the (001) surface in which the value is slightly lower.

A schematic diagram of the relative position of the VB and CB for the (110) and (010) surface for TiO_2, SnO_2, $TiO_2/SnO_2/TiO_2$ and $SnO_2/TiO_2/SnO_2$ systems can be found in Figure 4a,b, respectively. In Figure 4a we can see that the bottom of the CB of the bare TiO_2 and SnO_2 (110) surfaces have very close energy values but the top of VB of the SnO_2 has a higher energy value than the TiO_2. In Figure 4b we can observe that the bare SnO_2 (010) surface presents the top of the VB as well as the bottom of CB at lower energy values than the bare TiO_2. These results

also have been found for the bulk SnO_2 and TiO_2 metal oxides (see Figure 2 in Zakrzewska and Radecka[48]). In addition, there is a stabilization of both the top of the VB and the bottom of CB in the $SnO_2/TiO_2/SnO_2$ (010) composite in relation to the bare TiO_2 (010) whereas an opposite trend is found for the $TiO_2/SnO_2/TiO_2$ (010) system. A similar behavior is found for (110) surface.

IV. Conclusions

We have clarified the interfacial and surface structures of $TiO_2/SnO_2/TiO_2$ and $SnO_2/TiO_2/SnO_2$ model systems by means of density functional theory calculations at B3LYP computing level. The surface energy, relative stability, structural and electronic properties of the (110), (010), (001) and (101) low index surfaces of bare TiO_2 and SnO_2 as well as the $TiO_2/SnO_2/TiO_2$ and $SnO_2/TiO_2/SnO_2$ composite systems have been obtained. The main results can be summarized as follows:

(1) The order of the energy increasing from the calculated data of bare TiO_2 and SnO_2 systems follows the sequence (110) < (010) < (101) < (001), whereas for $SnO_2/TiO_2/SnO_2$ and $TiO_2/SnO_2/TiO_2$ it is (010) < (101) < (110) < (001) and (010) ≈ (110) < (101) < (001), respectively.

(2) The composite $SnO_2/TiO_2/SnO_2$ system has a higher surface energy than the individual SnO_2 and TiO_2 oxides whereas for the $TiO_2/SnO_2/TiO_2$ the corresponding values are of the same order that the TiO_2 oxide and lower than those of SnO_2 oxide.

(3) The stabilization of (010) surface for $SnO_2/TiO_2/SnO_2$ composite system can be associated with the fact that the more open and corrugated structure of the (010) surface allows the large Sn atoms of the SnO_2 layer to accommodate better than the (110) one on the respective TiO_2 cores.

(4) The Ti atoms of the TiO_2 (010) and (110) layers show similar ability to accommodate on the SnO_2 cores of the $TiO_2/SnO_2/TiO_2$ composite system, due to their small size when compared with the Sn ones.

(5) The relaxation of the surfaces in the *z*-direction seems to follow a general behavior for both $SnO_2/TiO_2/SnO_2$ and $TiO_2/SnO_2/TiO_2$ systems that have to accommodate the lattice mismatch between the TiO_2 and the SnO_2, i.e., pronounced displacements outward for the SnO_2 on TiO_2 and inward for the TiO_2 on SnO_2 for all the surfaces.

(6) In both $SnO_2/TiO_2/SnO_2$ and $TiO_2/SnO_2/TiO_2$ composite systems, the main characteristics of the upper VBs for all the studied surfaces are dominated by the external layers, i.e., by the SnO_2 and the TiO_2, respectively, whereas the bottom of the CBs are located at the same points of the first Brillouin zone than their corresponding cores, i.e., TiO_2 and SnO_2, respectively; the exception to this rule is the (001) $TiO_2/SnO_2/TiO_2$ surface in which the bottom of CB is located at Γ instead of at M as in the bare TiO_2.

(7) There is an energy stabilization of both VB top and CB bottom for (110) surface of the $SnO_2/TiO_2/SnO_2$ composite system in relation to the core TiO_2, but an opposite trend is found for the (110) surface of the $TiO_2/SnO_2/TiO_2$ composite system in relation to the core SnO_2. A similar behavior is found for (010) surface of both composite systems.

(8) Our results may explain the growth of the $TiO_2@SnO_2$ bimorph composite nanotapes experimentally reported in which the TiO_2 is epitaxially oriented on the side (010) surface.

With this work, we hope to provide results that will be useful for studies on $TiO_2/SnO_2/TiO_2$ and $SnO_2/TiO_2/SnO_2$ composite systems and for future investigations of the physics/chemistry of their surfaces as well.

Acknowledgment. This work was supported Spanish Fundació Bancaixa (project P1 1B2005-20) and Brazilian funding: FAPESP and CNPq. JRS thanks Spanish Generalitat Valenciana and Fundació Bancaixa for fellowships as invited professor.

References and Notes

(1) Pan, Z. W.; Dai, Z. R.; Wang, Z. L. *Science* **2001**, *291*, 1947.
(2) Huang, M. H.; Mao, S.; Feick, H.; Yan, H.; Wu, Y.; Kind, H.; Weber, E.; Russo, R. *Science* **2001**, *292*, 1897.
(3) Comini, E.; Faglia, G.; Sberveglieri, G.; Pan, Z.; Wang, Z. L. *Appl. Phys. Lett.* **2002**, *81*, 1869.
(4) Law, M.; Kind, H.; Messer, B.; Kim, F.; Yang, P. *Angew. Chem.* **2002**, *114*, 2511.
(5) Law, M.; Sirbuly, D. J.; Johnson, J. C.; Goldberger, J.; Saykally, R. J.; Yang, P. *Science* **2004**, *305*, 1269.
(6) Narayanan, R.; El-Sayed, M. A. *J. Phys. Chem. B* **2005**, *109*, 12663.
(7) Rao, C. N. R.; Müller, A.; Cheetham, A. K. *The Chemistry of Nanomaterials. (Synthesis, Properties and Applications)*; Wiley-VCH: Weinheim, 2005.
(8) He, J. H.; Wu, T. H.; Hsin, C. L.; Li, K. M.; Chen, L. J.; Chueh, Y. L.; Chou, L. J.; Wang, Z. L. *Small* **2006**, *2*, 116.
(9) Aprile, C.; Corma, A.; Garcia, H. *Phys. Chem. Chem. Phys.* **2008**, *10*, 769.
(10) Zakrzewska, K. *Thin Solid Films* **2001**, *391*, 229.
(11) Ertl, G.; Knözinger, H.; Schüth, F.; Weitkamp, J. *Handbook of Heterogeneous Catalysis*; Wiley-VCH: Weinheim, 1997.
(12) van Santen, R. A.; Neurock, M. *Molecular Heterogeneous Catalysis (A Conceptual and Computational Approach)*; Wiley-VCH: Weinheim, 2006.
(13) Wua, R.-J.; Chena, C.-Y.; Chena, M.-H.; Sun, Y.-L. *Sens. Actuators B* **2007**, *123*, 1077.
(14) Yu, H.-C.; Shen, P. *J. Eur. Ceram. Soc.* **2008**, *28*, 91.
(15) Yang, J.; Li, D.; Wang, X.; Yang, X.; Lu, L. *Solid State Chem.* **2002**, *165*, 193.
(16) Kanai, N.; Nuida, T.; Ueta, K.; Hashimoto, K.; Watanabe, T.; Ohsaki, H. *Vacuum* **2004**, *74*, 723.
(17) Lee, H. C.; Hwang, W. S. *Appl. Surf. Sci.* **2006**, *253*, 1889.
(18) Kubo, T.; Sayama, K.; Nozoye, H. *J. Am. Chem. Soc.* **2006**, *128*, 4074.
(19) Chinarro, E.; Moreno, B.; Jurado, J. R. *J. Eur. Ceram. Soc.* **2007**, *27*, 3601.
(20) Fahmi, A.; Minot, C.; Silvi, B.; Causa, M. *Phys. Rev. B* **1993**, *47*, 11717.
(21) Ramamoorthy, M.; Vanderbilt, D.; King-Smith, R. D. *Phys. Rev. B* **1994**, *49*, 16721.
(22) Oviedo, J.; Gillan, M. J. *Surf. Sci.* **2000**, *463*, 93.
(23) Maki-Jaskari, M. A.; Rantala, T. T. *Phys. Rev. B* **2001**, *64*, 075407.
(24) Diebold, U. *Surf. Sci. Rep.* **2003**, *48*, 53.
(25) Bouzoubaa, A.; Markovits, A.; Calatayud, M.; Christian, M. *Surf. Sci.* **2005**, *583*, 107.
(26) Batzill, M.; Diebold, U. *Prog. Surf. Sci.* **2005**, *79*, 47.
(27) Beltrán, A.; Gracia, L.; Andrés, J. *J. Phys. Chem. B* **2006**, *110*, 23417.
(28) Di Valentin, C.; Pacchioni, G.; Selloni, A. *Phys. Rev. Lett.* **2006**, *97*, 166803.
(29) Gong, X.-Q.; Selloni, A. *Phys. Rev. B* **2007**, *76*, 235307.
(30) Mitev, P. D.; Hermansson, K. *Surf. Sci.* **2007**, *601*, 5359.
(31) Krüger, P.; Bourgeois, S.; Domenichini, B.; Magnan, H.; Chandesris, D.; Le Fèvre, P.; Flank, A. M.; Jupille, J.; Floreano, L.; Cossaro, A.; Verdini, A.; Morgante, A. *Phys. Rev. Lett.* **2008**, *100*, 055501.
(32) Labat, F.; Baranek, P.; Adamo, C. *J. Chem. Theory Comput.* **2008**, *4*, 341.
(33) Duan, Y. *Phys. Rev. B* **2008**, *77*, 045332.
(34) Okada, M.; Yamada, Y.; Yoshimura, K. *Surf. Sci.* **2006**, *600*, 4385.
(35) Ohsaki, H.; Kanai, N.; Fukunaga, Y.; Suzuki, M.; Watanabe, T.; Hashimoto, K. *Thin Solid Films* **2006**, *502*, 138.
(36) Kunst, M.; Moehl, T.; Wunsch, F.; Tributsch, H. *Superlattices Microstruct.* **2006**, *39*, 376.
(37) Akurati, K. K.; Vital, A.; Hany, R.; Bommer, B.; Graule, T.; Winterer, M. *Int. J. Photoenergy* **2005**, *7*, 153.
(38) Chen, S. F.; Chen, L.; Gao, S.; Cao, G. Y. *Mater. Chem. Phys.* **2006**, *98*, 116.
(39) Liu, P.; Zhou, T. Y.; Lin, H. X.; Fu, X. Z. *Acta Phys.-Chim. Sinica* **2001**, *17*, 265.
(40) Chai, S. Y.; Kim, Y. S.; Lee, W. I. *J. Electroceram.* **2006**, *17*, 323.
(41) Tada, H.; Hattori, A.; Tokihisa, Y.; Imai, K.; Tohge, N.; Ito, S. *J. Phys. Chem. B* **2000**, *104*, 4585.
(42) Ribeiro, C.; Longo, E.; Leite, R. E. *Appl. Phys. Lett.* **2007**, *91*, 103105.

(43) He, R.; Law, M.; Fan, R.; Kim, F.; Yang, P. *Nano Lett.* **2002**, *2*, 1109.
(44) Hou, L. R.; Yuan, C. Z.; Peng, Y. *J. Hazardous Mater.* **2007**, *139*, 310.
(45) Liu, Z. Y.; Sun, D. D. L.; Guo, P.; Leckie, J. O. *Nano Lett.* **2007**, *7*, 1081.
(46) Zakrzewska, K.; Brudnik, A.; Radecka, M.; Posadowski, W. *Thin Solid Films* **1999**, *344*, 152.
(47) Zakrzewska, K.; Radecka, A.; Przewoznik, J.; Kowalski, K.; Czuba, P. *Thin Solid Films* **2005**, *490*, 101.
(48) Zakrzewska, K.; Radecka, M. *Thin Solid Films* **2007**, *515*, 8332.
(49) Sensato, F. R.; Custodio, R.; Longo, E.; Beltrán, A.; Andrés, J. *Catal. Today* **2003**, *85*, 145.
(50) Sambrano, J. R.; Nobrega, G. F.; Taft, C. A.; Andrés, J.; Beltrán, A. *Surf. Sci.* **2005**, *580*, 71.
(51) Dovesi, R.; Saunders, V. R.; Roetti, C.; Orlando, R.; Zicovich-Wilson, C. M.; Pascale F.; Civalleri B.; Doll, K.; Harrison, N. M.; Bush, I. J.; D'Arco, Ph.; Llunell, M. *CRYSTAL06 User's Manual*; University of Torino, 2006.
(52) Rassolov, V. A.; Pople, J. A.; Ratner, M. A.; Windus, T. L. *J. Chem. Phys.* **1998**, *109*, 1223.
(53) Beltrán, A.; Sambrano, J. R.; Calatayud, M.; Sensato, F. R.; Andrés, J. *Surf. Sci.* **2001**, *490*, 116.
(54) Calatayud, M.; Mori-Sanchez, P.; Beltrán, A.; Pendás, A. M.; Francisco, E.; Andrés, J.; Recio, J. M. *Phys. Rev. B* **2001**, *64*, 184113.
(55) Available at http://www.crystal.unito.it/.
(56) Durand, P.; Barthelat, J. C. *Theor. Chim. Acta* **1975**, *38*, 283.
(57) Becke, A. D. *J. Chem. Phys.* **1993**, *98*, 5648.
(58) Lee, C.; Yang, W.; Parr, R. G. *Phys. Rev. B* **1988**, *37*, 785.
(59) Hu, C. H.; Chong, D. P. *Encyclopedia of Computational Chemistry*; Wiley: Chichester, U.K., 1998.
(60) Sensato, F. R.; Custodio, R.; Calatayud, M.; Beltrán, A.; Andrés, J.; Sambrano, J. R.; Longo, E. *Surf. Sci.* **2002**, *511*, 408.
(61) Bredow, T.; Giordano, L.; Cinquini, F.; Pacchioni, G. *Phys. Rev. B* **2004**, *70*, 035419.
(62) Thompson, S. J.; Lewis, S. P. *Phys. Rev. B* **2006**, *73*, 073403.
(63) Oviedo, J.; Gillan, M. J. *Surf. Sci.* **2002**, *513*, 26.
(64) Fiorentini, V.; Methfessel, M. *J. Phys.: Condens. Mater* **1996**, *8*, 6525.
(65) Marlo, M.; Milman, V. *Phys. Rev. B* **2000**, *62*, 2899.
(66) Beltrán, A.; Andrés, J.; Longo, E.; Leite, E. R. *Appl. Phys. Lett.* **2003**, *83*, 635.
(67) Barnard, A. S.; Zapol, P. *Phys. Rev. B* **2004**, *70*, 235403.
(68) Perron, H.; Domain, C.; Roques, J.; Drot, R.; Simoni, E.; Cantalette, H. *Theor. Chem. Acc.* **2007**, *117*, 565.
(69) Lin, W.; Zhang, Y. F.; Li, Y.; Ding, K. N.; Li, J. Q.; Xu, Y. J. *J. Chem. Phys.* **2006**, *124*, 054704.
(70) Cox, P. A. *Transition Metal Oxides - An Introduction to Their Electronic Structure*; Clarendon: Oxford, U.K., 1992.
(71) Pascual, J.; Camassel, J.; Mathieu, H. *Phys. Rev. B* **1978**, *18*, 5606.
(72) Vos, K.; Krusemeyer, H. J. *J. Phys. C-Solid State Phys.* **1977**, *10*, 3893.
(73) Soratin, P. I.; Schwarz, K. *Inorg. Chem.* **1992**, *31*, 567.
(74) Haines, J.; Leger, J. M. *Phys. Rev. B* **1997**, *55*, 11144.
(75) Agekyan, V. T. *Phys. Status Solidi (a)* **1977**, *43*, 11.
(76) Dawar, A. L.; Joshi, J. C. *J. Mater. Sci.* **1984**, *19*, 1.
(77) Bolzan, A. A.; Fong, C.; Kennedy, B. J.; Howard, C. J. *Acta Crystallogr. B* **1997**, *53*, 373.
(78) Calatayud, M.; Andrés, J.; Beltrán, A. *Surf. Sci.* **1999**, *430*, 213.
(79) Gracia, L.; Beltrán, A.; Andrés, J. *J. Phys. Chem. B* **2007**, *111*, 6479.
(80) Mulheran, P. A.; Harding, J. H. *Mol. Sim. Mater. Sci. Eng.* **1992**, *1*, 39.
(81) Slater, B.; Catlow, C. R.; Gay, D. H.; Williams, D. E.; Dusastre, V. *J. Phys. Chem. B* **1999**, *103*, 10644.

JP801604N